Nonlocal Density Functional Theory and Grand Canonical Monte Carlo Molecular Simulations of Water Adsorption in Confined Media

ARTICLE *in* THE JOURNAL OF PHYSICAL CHEMISTRY C · OCTOBER 2014

Impact Factor: 4.77 · DOI: 10.1021/jp505239e

5 AUTHORS, INCLUDING:

Carine Malheiro
Université de Pau et des Pays de l'Adour
5 PUBLICATIONS **7** CITATIONS
SEE PROFILE

Christelle Miqueu
Université de Pau et des Pays de l'Adour
35 PUBLICATIONS **483** CITATIONS
SEE PROFILE

AIP | The Journal of Chemical Physics

Density functional theory for the description of spherical non-associating monomers in confined media using the SAFT-VR equation of state and weighted density approximations

Carine Malheiro, Bruno Mendiboure, Frédéric Plantier, Felipe J. Blas, and Christelle Miqueu

Citation: The Journal of Chemical Physics **140**, 134707 (2014); doi: 10.1063/1.4869996
View online: http://dx.doi.org/10.1063/1.4869996
View Table of Contents: http://scitation.aip.org/content/aip/journal/jcp/140/13?ver=pdfcov
Published by the AIP Publishing

Density functional theory for the description of spherical non-associating monomers in confined media using the SAFT-VR equation of state and weighted density approximations

Carine Malheiro,[1] Bruno Mendiboure,[1] Frédéric Plantier,[1] Felipe J. Blas,[2] and Christelle Miqueu[1]

[1]*Université Pau et Pays Adour, CNRS, TOTAL - UMR 5150 – LFC-R – Laboratoire des Fluides Complexes et leurs Réservoirs, BP 1155 – PAU, F-64013, France*

[2]*Departamento de Física Aplicada, and Centro de Física Teórica y Matemática FIMAT, Universidad de Huelva, 21071 Huelva, Spain*

(Received 17 January 2014; accepted 19 March 2014; published online 7 April 2014)

As a first step of an ongoing study of thermodynamic properties and adsorption of complex fluids in confined media, we present a new theoretical description for spherical monomers using the Statistical Associating Fluid Theory for potential of Variable Range (SAFT-VR) and a Non-Local Density Functional Theory (NLDFT) with Weighted Density Approximations (WDA). The well-known Modified Fundamental Measure Theory is used to describe the inhomogeneous hard-sphere contribution as a reference for the monomer and two WDA approaches are developed for the dispersive terms from the high-temperature Barker and Henderson perturbation expansion. The first approach extends the dispersive contributions using the scalar and vector weighted densities introduced in the Fundamental Measure Theory (FMT) and the second one uses a coarse-grained (CG) approach with a unique weighted density. To test the accuracy of this new NLDFT/SAFT-VR coupling, the two versions of the theoretical model are compared with Grand Canonical Monte Carlo (GCMC) molecular simulations using the same molecular model. Only the version with the "CG" approach for the dispersive terms provides results in excellent agreement with GCMC calculations in a wide range of conditions while the "FMT" extension version gives a good representation solely at low pressures. Hence, the "CG" version of the theoretical model is used to reproduce methane adsorption isotherms in a Carbon Molecular Sieve and compared with experimental data after a characterization of the material. The whole results show an excellent agreement between modeling and experiments. Thus, through a complete and consistent comparison both with molecular simulations and with experimental data, the NLDFT/SAFT-VR theory has been validated for the description of monomers.
 [http://dx.doi.org/10.1063/1.4869996]

I. INTRODUCTION

Understanding the thermodynamic properties and adsorption phenomena of extremely confined fluids has a great interest not solely in terms of knowledge but also for many practical and industrial applications such as, for instance, storage of natural gas[1] and hydrogen,[2] carbon dioxide capture,[3] exploitation of non-conventional resources such as coal bed methane,[4] etc. Hence, for several years, substantial efforts have been dedicated to the development of on the one hand molecular simulations and theoretical models and on the other hand experimental techniques to study the properties of confined fluids.

Among the theoretical developments, density functional theory (DFT) has emerged as one of the most powerful and convenient molecular approach for the description of the thermodynamic properties of inhomogeneous fluids. DFT approaches retain detailed information of the microstructure of heterogeneous fluids but with a much less computational expense than molecular simulations. Comprehensive description of DFT and its applications can be found for instance in the reviews of Evans,[5] Wu,[6,7] Emborski *et al.*,[8] Landers *et al.*,[9] and the monography of Davis.[10] DFT for systems involving both repulsive and attractive forces is usually defined by its intrinsic Helmholtz free energy functional, which is normally approximated as a perturbation about a hard-sphere reference system. Different options for both the hard sphere term and the attractive contribution exist in the literature (see reviews mentioned above). Among the various DFT approaches, some based on the Wertheim's thermodynamic perturbation theory (TPT1)[11,12] have been proposed recently. These versions can take the advantage of reducing to the Statistical Associating Fluid Theory (SAFT) equation of state[13,14] in the bulk limit and thus to provide a uniform efficient platform to describe simultaneously the thermodynamic properties of homogeneous and heterogeneous states of realistic fluids. Several of these works have concerned fluid interfaces. In that case, local density approximations (LDA) were used in the DFT and proved to be efficient to describe the smooth density gradients appearing in such interfaces. Among these studies, Jackson and co-workers have proposed a statistical associating fluid theory for potential of variable range (SAFT-VR)/DFT formalism to predict the properties of vapour-liquid and liquid-liquid interfaces of complex (non-associating, chains, associating, etc.) fluids and their mixtures.[15–20] Kahl and Winkelman[21] have used a PT-LJ-SAFT/DFT approach to compute the vapor

liquid equilibria and interfacial properties of non-associating hydrocarbon fluids and von Müller *et al.*[22] obtained the surface tension of alkanes, ethers, and aromates with a PCP-SAFT/DFT formalism. The LDA is suitable for the description of fluid interfaces but is not adapted for the case of confined fluids. Indeed, in the case of strong density heterogeneities, an accurate description of the system needs a non-local treatment of DFT (NLDFT) with the use of Weighted Density Approximations (WDA). This latter can be done using theories such as Fundamental Measure Theory (FMT)[23] and its derivations[24–27] or others that treat the density as a non-local space function[10]. Such NLDFT/SAFT coupling was also applied to fluid interfaces.[28–31] But some works have been recently dedicated to fluids near solid surfaces or confined in slit pores. Ye *et al.*[32,33] have used SW potentials in their DFT for homopolymers and copolymers confined in nanoslit pores. Shen *et al.*[34,35] have developed a PC-SAFT/DFT for the description of the behavior of fluids confined in slit micropores and Schindler *et al.*[36] have modeled very recently the adsorption of chain molecules in slit-shaped pores with a SAFT-FMT-DFT approach. Among the outstanding works on SAFT/DFT coupling, one has to mention also the development of interfacial SAFT (iSAFT) by Chapman and co-workers for the description of interfacial properties and adsorption of chain fluids.[37–40]

In this article, we present an original coupling between a new non-local version of DFT and the SAFT-VR version of the well-known Statistical Associating Fluid Theory for the description of the inhomogeneous behavior of fluids in highly confined media. The present work is a first step of an ongoing NLDFT/SAFT-VR coupling. It focuses on the monomer contribution and especially in the way to extend the dispersive terms of the monomer contribution of SAFT-VR in the NLDFT formalism. Two versions of the theory are developed in this work. In order to test their accuracy, Grand Canonical Monte Carlo simulations are also performed. Finally, the new formalism is used to predict the adsorption behavior of methane on a real carbon adsorbent, the Carbon Molecular Sieve (CMS) Carboxen 1012 and a consistent comparison is made with experimental adsorption isotherms at the same thermodynamics conditions, once the material has been characterized.

The rest of the article is organized as follows. Section II gives the basis of the new model combining NLDFT and SAFT-VR. Then, Sec. III deals with the results and discussions. First, the theoretical study at pore scale by the development of a new model is compared to Grand Canonical Monte Carlo (CGMC) molecular simulations. Then, the comparison of the modeled adsorbed quantities is made with experimental adsorption isotherms using a magnetic suspension microbalance device on the activated carbon Carboxen 1012 at the same conditions of temperature and pressure. Finally, Sec. IV is devoted to the conclusions of this work.

II. THEORY

We consider a system at temperature T, chemical potential μ in a volume V. In an external potential $V_{ext,}$ the grand potential Ω of the inhomogeneous fluid is assumed to be a functional of the molecular density $\rho(\mathbf{r})$ in the framework of the DFT[5]

$$\Omega\left[\rho(\mathbf{r})\right] = A\left[\rho(\mathbf{r})\right] + \int d\mathbf{r}\rho(\mathbf{r})\left\{V_{ext}(\mathbf{r}) - \mu\right\}, \tag{1}$$

where A[$\rho(\mathbf{r})$] is the Helmholtz free energy.

The equilibrium density distribution is calculated through the minimization of the grand potential by solving the corresponding Euler-Lagrange equation[5]

$$\frac{\delta\Omega\left[\rho(\mathbf{r})\right]}{\delta\rho(\mathbf{r})} = \frac{\delta A\left[\rho(\mathbf{r})\right]}{\delta\rho(\mathbf{r})} + V_{ext}(\mathbf{r}) - \mu = 0. \tag{2}$$

To express the Helmholtz free energy A of the fluid and its associated chemical potential μ, the SAFT-VR theory[41] is used herein,

$$A = A^{ideal} + A^{mono} + A^{chain} + A^{assoc}, \tag{3}$$

where A^{ideal} is the ideal free energy, A^{mono} is the monomer free energy taking into account the dispersive contributions and is the sum of a reference hard-sphere term and a high-temperature Barker and Henderson[42,43] perturbation expansion at second order $A^{mono} = A^{HS} + A_1 + A_2$, A^{chain} is the free energy due to the formation of a chain molecule, and A^{assoc} is the association free energy.

In this work, we consider fluids of non-associating spherical monomers of diameter σ with a mean-field (MF) approximation, so we do not consider chain and associating contributions. Thus, we follow the SAFT-VR MF DFT development of Gloor and co-workers[17] in which the correlations due to the long-range attractive interactions are neglected. In that case, the first-order monomer perturbation is partitioned to get on the one hand the "short-range" contribution A_1^{sr} and on the other hand the "long-range" contribution that becomes the classical attractive term A^{att} in the DFT.[17]

Thus, in the MF approximation, the NLDFT/SAFT-VR Helmholtz free energy functional is given by[17]

$$A\left[\rho\left(\mathbf{r}\right)\right] = A^{ideal}\left[\rho\left(\mathbf{r}\right)\right] + A^{HS}\left[\rho\left(\mathbf{r}\right)\right] + A^{att}\left[\rho\left(\mathbf{r}\right)\right] + A_1^{sr}\left[\rho\left(\mathbf{r}\right)\right] + A_2\left[\rho\left(\mathbf{r}\right)\right]. \tag{4}$$

A. Ideal contribution

The ideal part A^{ideal} $[\rho(\mathbf{r})]$ is the exactly known term given by[5]

$$A^{ideal}\left[\rho(\mathbf{r})\right] = k_B T \int d\mathbf{r}\rho(\mathbf{r})[\ln(\rho(\mathbf{r})\Lambda^3) - 1], \tag{5}$$

where k_B is the Boltzmann constant and Λ is the de Broglie thermal wavelength of the molecules forming the system.

B. Hard-sphere contribution

The hard-sphere free energy is treated non-locally using a weighted density approximation. Here, the Modified Fundamental Measure Theory (MFMT)[44] has been selected because the free-energy reduces to the Carnahan-Starling equation of state[45] in the bulk limit just as the hard-sphere contribution in the SAFT-VR theory. This WDA provides six scalar and

vector weighted densities $n_\alpha(\mathbf{r})$,

$$n_\alpha(\mathbf{r}) = \int d\mathbf{r}'\rho(\mathbf{r}')w^{(\alpha)}(\mathbf{r}' - \mathbf{r}), \tag{6}$$

where $\alpha = 0$, 1, 2, 3, v_1, and v_2, and the weighted functions $w^{(\alpha)}(\mathbf{r})$ are given by

$$w^{(2)}(\mathbf{r}) = \pi\sigma^2 w^{(0)}(\mathbf{r}) = 2\pi\sigma\, w^{(1)}(\mathbf{r}) = \delta\left(\frac{\sigma}{2} - r\right), \tag{7}$$

$$w^{(3)}(\mathbf{r}) = \Theta\left(\frac{\sigma}{2} - r\right), \tag{8}$$

$$\mathbf{w}^{v2}(\mathbf{r}) = 2\pi\,\mathbf{w}^{v1}(\mathbf{r}) = \left(\frac{\mathbf{r}}{r}\right)\delta\left(\frac{\sigma}{2} - r\right), \tag{9}$$

where $\delta(r)$ is the Dirac delta function and $\Theta(r)$ is the Heaviside step function.

Then, the hard-sphere Helmholtz free energy is given by[44]

$$A^{HS}[\rho(\mathbf{r})] = k_B T \int dr[\Phi^{HS(s)}\{n_\alpha(\mathbf{r})\} + \Phi^{HS(v)}\{n_\alpha(\mathbf{r})\}], \tag{10}$$

where

$$\Phi^{HS(s)}\{n_\alpha(\mathbf{r})\} = -n_0\ln(1-n_3) + \frac{n_1 n_2}{1-n_3} + \frac{{n_2}^3\ln(1-n_3)}{36\pi {n_3}^2} + \frac{{n_2}^3}{36\pi n_3(1-n_3)^2} \tag{11}$$

is the scalar part and

$$\Phi^{HS(v)}\{n_\alpha(\mathbf{r})\} = -\frac{\mathbf{n}_{v1}\cdot\mathbf{n}_{v2}}{1-n_3} - \frac{n_2\mathbf{n}_{v2}\cdot\mathbf{n}_{v2}\ln(1-n_3)}{12\pi {n_3}^2} - \frac{n_2\mathbf{n}_{v2}\cdot\mathbf{n}_{v2}}{12\pi n_3\ln(1-n_3)^2} \tag{12}$$

is the vector part.

C. Dispersive contributions

The attractive contribution A^{att} takes into account the long-range attractive interactions under the well-know mean-field approximation,[5] i.e., the correlations between molecules are neglected in the attractive interactions. This contribution is given by

$$A^{att}[\rho(\mathbf{r})] = \frac{1}{2}\int d\mathbf{r}\rho(\mathbf{r})\int d\mathbf{r}'\rho(\mathbf{r}')\Phi^{att}(|\mathbf{r}-\mathbf{r}'|), \tag{13}$$

where $\Phi^{att}(|\mathbf{r}-\mathbf{r}'|)$ is, in this work, the attractive part of the square-well (SW) potential with a depth ε and a range λ used in the SAFT-VR equation of state

$$\Phi^{att}(r) = u^{SW}(r,\sigma,\lambda) = \begin{cases} -\varepsilon & if\ \sigma < r < \lambda\sigma \\ 0 & elsewhere \end{cases}. \tag{14}$$

For the dispersive terms $A_1{}^{sr}$ and A_2, we propose two approaches to treat this contribution non-locally.

1. "FMT" approach

The first method applies the weighted densities defined in the FMT with the dispersive terms $A_1{}^{sr}[\rho(r)]$ and $A_2[\rho(r)]$. In that case, the short-range contribution may be written as

$$A_1^{sr,FMT}[\rho(\mathbf{r})] = -\alpha^{VdW}\int d\mathbf{r}\rho(\mathbf{r})\, a_1^{sr,FMT}(\{n_\alpha(\mathbf{r})\}), \tag{15}$$

where α^{VdW} is given by

$$\alpha^{VdW} = \frac{2\pi}{3}\sigma^3\varepsilon(\lambda^3 - 1). \tag{16}$$

In the original SAFT-VR MF DFT formalism,[17] the free-energy $A_1{}^{sr}[\rho(r)]$ that contributes to the short-range part of the correlations due to the attraction is approximated in terms of bulk radial distribution function at a density evaluated locally. In this work, we follow a similar approach but with some important differences. This contribution is now written as

$$a_1^{sr,FMT}(\{n_\alpha(\mathbf{r})\}) = n_0(\mathbf{r})\,\xi(\mathbf{r})\left[g_{FMT}^{HS}\left(\sigma, \left\{n_\alpha^{eff}(\mathbf{r})\right\}\right) - 1\right]. \tag{17}$$

Here, we assume that the free energy is evaluated non-locally through a set of smooth functions. Following the work of Yu and Wu,[27] the radial distribution function is approximated by

$$g_{FMT}^{HS}(\sigma,\{n_\alpha(r)\}) = \frac{1}{1-n_3} + \frac{\sigma}{2}\frac{n_2\xi}{2(1-n_3)^2} + \left(\frac{\sigma}{2}\right)^2\frac{n_2^2\xi}{18(1-n_3)^3}, \tag{18}$$

where ξ is a position-dependent function that is written as

$$\xi(r) = 1 - \frac{\mathbf{n}_{v2}(\mathbf{r})\cdot\mathbf{n}_{v2}(\mathbf{r})}{{n_2}^2(r)}. \tag{19}$$

In the original SAFT-VR formalism,[41] the radial distribution function at contact length is evaluated at an effective packing fraction[41,46] (or density). Hence, we define smooth weighted densities in terms of the effective density ρ^{eff} of the system. They are given by

$$n_\alpha^{eff}(\mathbf{r}) = \int d\mathbf{r}\rho^{eff}(\mathbf{r})w^{(\alpha)}(\mathbf{r}\copyright - \mathbf{r}). \tag{20}$$

The second order perturbation term of our approach may be written as

$$A_2^{FMT}[\rho(\mathbf{r})] = \frac{1}{2}\frac{\varepsilon}{k_B T}\int d\mathbf{r}\rho(\mathbf{r})K_{FMT}^{HS}(\{n_\alpha(\mathbf{r})\})\,n_0(\mathbf{r})\,\xi(\mathbf{r}) \times \frac{\partial a_1^{FMT}(\{n_\alpha(\mathbf{r})\})}{\partial\rho(\mathbf{r})}, \tag{21}$$

where the a_1 contribution is written as

$$a_1^{FMT}(\{n_\alpha(\mathbf{r})\}) = -\alpha^{VdW}n_0(\mathbf{r})\,\xi(\mathbf{r})\,g_{FMT}^{HS}\left(\sigma,\left\{n_\alpha^{eff}(\mathbf{r})\right\}\right). \tag{22}$$

The original Percus-Yevick hard-sphere isothermal compressibility given in bulk phase[47] by

$$K^{HS} = \frac{\zeta_0(1-\zeta_3)^4}{\zeta_0(1-\zeta_3)^2 + 6\zeta_1\zeta_2(1-\zeta_3) + 9\zeta_2{}^3}, \tag{23}$$

where

$$\zeta_i = \frac{\pi}{6}\rho\sigma^i \tag{24}$$

is now transformed with the Hansen-Goos and Roth[48] and Yu and Wu[27] substitutions to be expressed with weighted densities in the following way:

$$K^{HS}_{FMT}(\{n_\alpha(\mathbf{r})\}) = \frac{\frac{\pi}{6}n_0(1-n_3)^4}{\frac{\pi}{6}n_0(1-n_3)^2 + \frac{\pi}{3}(n_1n_2 - \mathbf{n}_{v1}\cdot\mathbf{n}_{v2}) + \frac{1}{24}\left(n_2^3 - 3n_2\mathbf{n}_{v2}\cdot\mathbf{n}_{v2}\right)}. \tag{25}$$

2. Coarse-grained ("CG") approach

In this method, a coarse-grained approach is preferred to treat the density non-locally in the dispersive terms. This method has been previously used by Tarazona[49] in several works and more recently by Gross[29] to describe the chain contribution in a DFT/PC-SAFT formalism. The weighted density is now defined as

$$\overline{\rho}(\mathbf{r}) = \frac{3}{4\pi\sigma^3}\int d\mathbf{r}'\rho(\mathbf{r}')\Theta(\sigma - |\mathbf{r}-\mathbf{r}'|). \tag{26}$$

The short-range dispersive contribution to the Helmholtz free energy is now written as

$$A_1^{sr,CG}[\rho(\mathbf{r})] = -\alpha^{VdW}\int d\mathbf{r}\rho(\mathbf{r})a_1^{sr,CG}(\mathbf{r}), \tag{27}$$

where

$$a_1^{sr,CG}(r) = \overline{\rho}(r)[g^{HS}(\sigma,\overline{\eta}^{eff}) - 1] \tag{28}$$

and the radial distribution function at contact length is now evaluated at the weighted effective packing fraction and given by

$$g^{HS}(\sigma,\overline{\eta}^{eff}) = \frac{1-\frac{\overline{\eta}^{eff}}{2}}{(1-\overline{\eta}^{eff})^3}. \tag{29}$$

$\bar{\eta}^{eff}$ ($\bar{\eta}$, λ) is the effective packing fraction that can be found in the literature[41,46] and the weighted packing fraction is related to the weighted density by

$$\overline{\eta} = \frac{\pi}{6}\overline{\rho}\sigma^3. \tag{30}$$

The second-order perturbation term in the current version is written as

$$A_2^{CG}[\rho(\mathbf{r})] = \frac{1}{2}\frac{\varepsilon}{k_BT}\int d\mathbf{r}\rho(\mathbf{r})K^{HS}_{CG}(\overline{\eta}(\mathbf{r}))\overline{\rho}(\mathbf{r})\frac{\partial a_1^{CG}(\mathbf{r})}{\partial\overline{\rho}(\mathbf{r})}, \tag{31}$$

where

$$a_1^{CG}(\mathbf{r}) = -\alpha^{VdW}\overline{\rho}(\mathbf{r})[g^{HS}(\sigma,\overline{\eta}^{eff})] \tag{32}$$

and

$$K^{HS}_{CG}(\overline{\eta}(\mathbf{r})) = \frac{(1-\overline{\eta}(\mathbf{r}))^4}{1+4\overline{\eta}(\mathbf{r})+4\overline{\eta}(\mathbf{r})^2}. \tag{33}$$

III. RESULTS AND DISCUSSION

The NLDFT/SAFT-VR coupled theory has been tested at microscopic and macroscopic scales. First, we compare density profiles of monomers in slit-like pores with Grand-Canonical Monte-Carlo (GCMC) molecular simulations of SW monomers at different temperatures and pressures. The average density in the pore and the capillary condensation are also compared. Then, the model is applied to study the adsorption of supercritical methane in the Carboxen 1012 CMS and computed adsorption isotherms are compared to experimental ones after a characterization of the material.

A. Density profiles of square-well monomers in slit-like pores

1. Description of the pores and numerical procedure

We apply in this section the NLDFT/SAFT-VR to determine the adsorption behavior of monomers in slit-like micropores using the two methods described in Sec. II. We briefly recall here that only the dispersion terms are different in these approaches.

We consider the pore as two solid parallel graphitic surfaces at a distance of H from carbon-center to carbon-center. Its interaction parameters[50] are $\sigma_{ss} = 0.34$ nm and $\varepsilon_{ss}/k_B = 28$ K. The external potential applied on the fluid is the Steele's potential[51] "10-4-3" from both surfaces:

$$V_{ext}(z) = V_{sf}(z) + V_{sf}(H-z) \tag{34}$$

with

$$V_{sf}(z) = 2\pi\rho_s\varepsilon_{sf}\sigma_{sf}{}^2\Delta\left[\frac{2}{5}\left(\frac{\sigma_{sf}}{z}\right)^{10} - \left(\frac{\sigma_{sf}}{z}\right)^4 - \frac{\sigma_{sf}{}^4}{3\Delta(z+0.61\Delta)^3}\right], \tag{35}$$

where $\rho_s = 114$ molecules/m^3 is the density of graphite,[50] $\Delta = 0.335$ nm is the space between two layers of graphite constituting the wall[50] and σ_{sf} and ε_{sf} are the solid-fluid interaction parameters determined by Lorentz-Berthelot rules $\sigma_{sf} = (\sigma_{ss} + \sigma_{ff})/2$ and $\varepsilon_{sf} = (\varepsilon_{ss}\varepsilon_{ff})^{1/2}$ where σ_{ff} and ε_{ff} are the monomer parameters in the SAFT-VR theory.

We have used a Picard iterative method to calculate the density profiles at equilibrium, resolving Eq. (2). The pore was discretized with n points along the direction perpendicular to the planar surfaces with a constant grid spacing of 0.005 nm and the calculation was proceeded until the error $\frac{1}{n}\sum_{i=1}^{n}(\rho_i^{new} - \rho_i^{old})$ is equal or lower than 10^{-5}.

2. GCMC molecular simulation calculations

In addition to the theoretical predictions presented in Sec. III A 1, we have also determined the adsorption behavior of a SW monomer in model pores using Monte Carlo simulations in order to test the performance of the two approaches proposed above. We have used the Grand Canonical Ensemble in which the chemical potential, volume of the pore, and temperature are kept constant. The attempts to move, create, or destroy a molecule were done with equal probability. The system was equilibrated between 5×10^5 and 10^6 cycles before collecting data. After equilibration, the overall density in the pore was determined by averaging about 10^8 configurations. Although the chemical potential can be used as independent variable in adsorption studies, it is normally preferable to consider the pressure as control variable. We have performed independent GCMC simulations in the bulk phase to relate the chemical potential and pressure of the SW monomer, this later computed via the classical virial route modified to take account of the discontinuous interactions.[52] These simulations provide an equation of state to connect the pressure and chemical potential of the fluid, which is also useful to compare our theoretical results with experimental data taken from the literature. In these GCMC simulations, the potential parameters of the SW monomer and of the solid were the same as the ones used in DFT calculations.

3. Comparison of theoretical results and GCMC simulation for methane in graphitic slit-like pores

The comparison between NLDFT/SAFT-VR theory and GCMC calculations has been done with the methane as the SW monomer. Its interaction parameters[53] in the SAFT-VR theory are $\sigma_{ff} = 0.367$ nm, $\varepsilon_{ff}/k_B = 168.8$ K, and $\lambda = 1.444$. Figure 1 shows the density profiles of methane at T = 353 K and P = 6 MPa for several pore widths in the whole range of micropores, from ultra-micropores (H = 0.94 nm) to close to the mesopores region (H = 1.86 nm) obtained from both versions of the theory presented. They are compared in this figure to both the GCMC simulations performed in this work and to

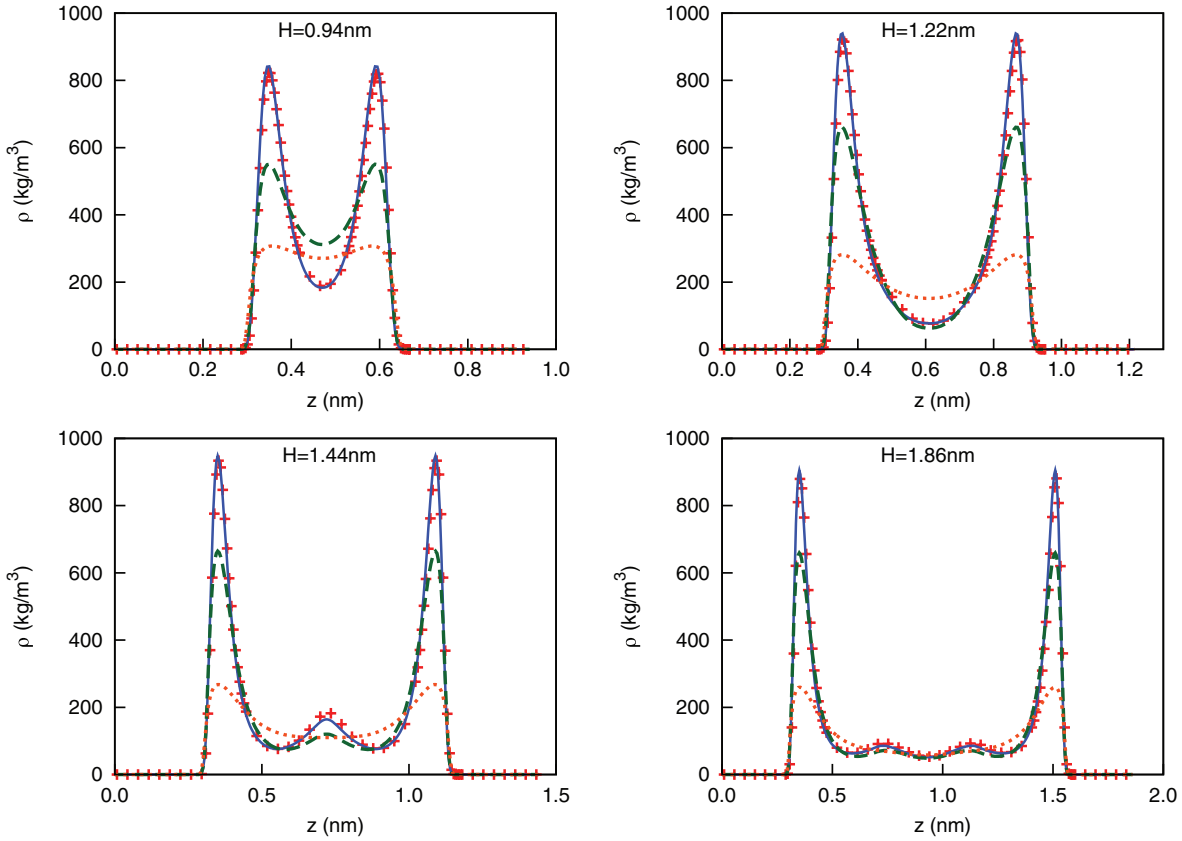

FIG. 1. Density profiles of methane in carbon slit pores at T = 353 K and P = 6 MPa with different pore sizes. The continuous curves are the "CG" version of the NLDFT/SAFT-VR modeling, the dashed lines are the "FMT" version of the NLDFT/SAFT-VR modeling, the dotted lines are LDA of DFT SAFT-VR theory and the symbols are the molecular simulation results.

the SAFT-VR DFT model of Gloor *et al.*[17] that uses a LDA. As it can be seen in Fig. 1, the number of peaks predicted by both NLDFT methods is identical to GCMC calculations and the location of the each peak is also well predicted. Although the "FMT" approach underestimates the density at the adsorption peaks, the "CG" approach gives an excellent description of the density profiles. Actually, the "FMT" dispersive contributions are negligible in relation to the HS contribution and thus, the predictions with the "FMT" approach are equivalent to the one of a repulsive fluid and underestimate the real structure. On the contrary, the dispersive contribution in the "CG" approach seems to be able to capture the real behavior of the confined monomer. Moreover, it can be seen that the LDA approach of the SAFT-VR DFT model cannot provide either the number of peaks, their position, and the density at adsorption peaks. As it could be suspected, a LDA is not adapted to the description of highly inhomogeneous fluids.

To get more information about the determination of adsorbed quantities in the pore with our model, we have determined for one of the pore sizes studied (H = 1.44 nm) the average density in the pore (that can be assimilated to the adsorbed quantity) at T = 313 K and T = 353 K for a large range of pressures in the supercritical region (from 0 up to 8 MPa). Figure 2 shows that the "CG" method fits very well the GCMC results in the whole range of pressures whereas the "FMT" approach gives good results for the lowest pressures (up to 1 MPa) but then underestimates the adsorbed quantities when the pressure increases. We can also see that the LDA approach of the DFT SAFT-VR model is not able to predict the average density in the pore even for low pressures.

Our results indicate that the "CG" method seems to provide a quantitative description of the thermodynamic and structural properties of monomers adsorbed in different pore widths at these temperatures for a large range of pressures compared to the GCMC molecular simulations. On the contrary, the "FMT" version of the theory fails to describe accurately both the structure of the monomers adsorbed in the pore and the adsorption isotherm at high pressures.

In order to test more deeply the adequacy of the "CG" approach in predicting the adsorption behavior of monomers in a large range of pore sizes, we have performed calculations to describe a discriminating phenomenon: the capillary condensation and its hysteresis. We have performed density profile calculations for adsorption and desorption of methane at T = 120 K for a pore of width H = 3.67 nm (mesopore region) and calculated the average density in the pore. At each pressure, the initial density distribution in the pore was the equilibrium density distribution of the previous pressure in order to mimic the experimental adsorption and desorption phenomena. Figure 3 represents the average density in the pore as a function of P/P_0 where P_0 is the saturation pressure of methane at 120 K. It shows that the "CG" approach of the NLDFT/SAFT-VR can describe the capillary condensation and evaporation that are metastable states of the phase transition and characteristic of experimental isotherms in mesopores. Moreover, the model allows finding the equilibrium capillary condensation transition. We can compare this transition with GCMC calculations. Indeed, in our GCMC calculation, the initial configurations were determined randomly so solely the equilibrium transition could be obtained. Figure 3 shows that NLDFT/SAFT-VR and GCMC results are fairly consistent.

We have also determined the density distribution of methane in the 3.67 nm pore at 120 K for two pressures: one before the capillary condensation (P/P_0 = 0.2) and one after, when the fluid is highly structured (P/P_0 = 0.8).

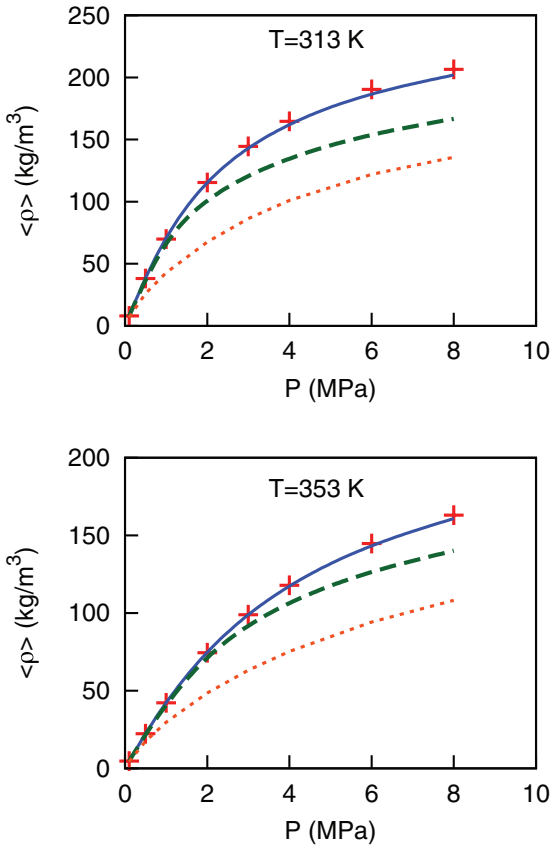

FIG. 2. Average density of methane in a carbon slit pore (H = 1.44 nm) at T = 313 K and T = 353 K. The continuous curves are the "CG" version of the NLDFT/SAFT-VR modeling, the dashed lines are the "FMT" version of the NLDFT/SAFT-VR modeling, the dotted lines are LDA of DFT SAFT-VR theory, and the symbols are the molecular simulation results.

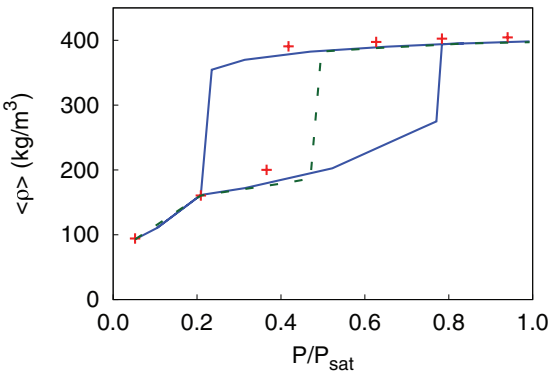

FIG. 3. Capillary condensation and evaporation of methane in a carbon slit-like pore of width 3.67 nm at 120 K. The continuous lines are the metastable states of capillary condensation and its hysteresis using the "CG" version of NLDFT/SAFT-VR. The dotted line (NLDFT/SAFT-VR) and the symbols (GCMC) are the equilibrium capillary condensation transition.

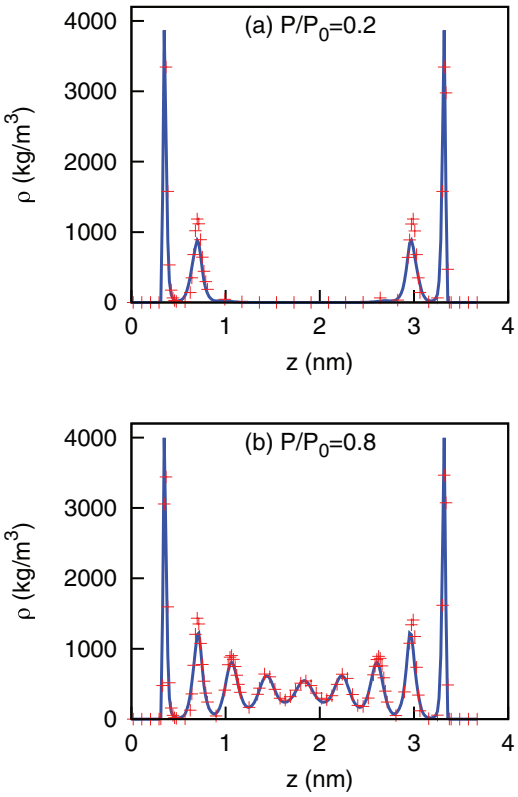

FIG. 4. Density profile of structured methane at 120 K on a carbon slit-like pore of 3.67 nm width before (a) and after (b) the capillary condensation. The continuous line is NLDFT/SAFT-VR results and the symbols are GCMC simulation results.

Figure 4 shows the comparison of these density profiles between the "CG" version of the theory and GCMC molecular simulations. For both profiles, one can see that the adsorption peaks are localized at the same position and density values are in good agreement between theory and simulations. In summary, the "CG" version of the NLDFT/SAFT-VR model is able to provide a very good description of the adsorption properties, not only for low-density states inside the pore but also for very dense and structured states.

B. Application to the determination of adsorption capacity of Carboxen 1012

In this section, we apply the "CG" version of the NLDFT/SAFT-VR theory to determine adsorption isotherms of methane (as the SW monomer) in a CMS.

1. Experimental description of adsorption isotherm measurement

Adsorption isotherms of pure methane were performed by means of a magnetic suspension microbalance (Rubotherm brand). The balance consists of a crucible suspended to a permanent magnet by a coupling system. The permanent magnet is kept in a suspension state due to the electromagnet. The force due to the mass uptake during the adsorption process is transmitted to the analytical balance by the magnetic suspension (coupling of the permanent magnet and electromagnet). Successive amounts of adsorbate are admitted in the adsorption chamber. After each admission, the pressure, the temperature, and the adsorbed mass are measured at regular intervals. Once the equilibrium is reached, the temperature, pressure, and mass signals are stored and a new amount of gas is admitted. However, as it is impossible to determine experimentally the volume of the adsorbed phase, the only available quantity is the excess mass m_{exc} defined as

$$m_{excess} = m_{ads} - \rho_{gas} V_{adsorbed}. \tag{36}$$

The overall uncertainty on the determination of the excess adsorbed mass is less than 0.5% over the entire range investigated in this study. More details on the measurement process can be found in another work.[54]

2. Materials

Experimental adsorption isotherms were carried out in a CMS sample, namely Carboxen 1012. This CMS was selected because in a recent paper, Mikhalovsky *et al.*[55] have shown on the one hand that this CMS is only microporous and on the other hand, from a comparison between the measured BET surface area and the one computed with the assumption that the pores are slit-like, that this CMS could be considered as made essentially of slit-like shaped pores. The Carboxen 1012 was supplied by Sigma Aldrich and methane adsorbate was provided by Linde Gas with a minimum purity of 99.995%.

3. Characterization of the microporous adsorbent

Carboxen 1012 is a microporous molecular sieve (pore widths < 2 nm). In order to have a relevant comparison between experimental and modeling adsorption isotherms, one needs first to get the Pore Size Distribution (PSD) of the material. In a previous work,[56] we have developed a new thermodynamic model in the same spirit of Horwath and Kawazoe approach[57] in order to link the filling pressure of a micropore to its size and thus obtain the PSD of a microporous carbon adsorbent from a low temperature adsorption isotherm (Nitrogen or Argon, classically). Here, we have performed the adsorption isotherm with nitrogen at 77.4 K on Carboxen 1012 with a Micromeretics gas porosimeter (ASAP 2020) (Figure 5) and then applied our model to get its PSD that is shown in Figure 6.

4. Adsorption isotherms of methane on Carboxen 1012

Experimental methane adsorption isotherms were measured at 313 K and 353 K at several pressures between 0.1 and 9 MPa. The results obtained are presented in Figure 7.

We have also predicted modeled adsorption isotherms using the "CG" version of NLDFT/SAFT-VR theory as the comparison with GCMC calculations has shown its efficiency. We have determined, at each pressure P, the density profile in each pore i of the Carboxen 1012 according to the partition of pore sizes obtained with the PSD (see Figure 6). Assuming the approximation most commonly used in the literature for

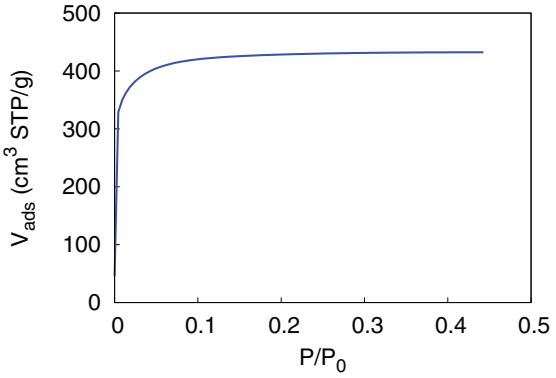

FIG. 5. Adsorption isotherm of N2 at 77.4 K on Carboxen 1012.

these kind of adsorbent materials, i.e., the porous material is approximated by a collection of individual micropores with planar or slit-like geometry (see also Sec. III B 2 – for the description of the Carboxen 1012 carbon sample), the excess adsorbed quantity that mimics the experimental measured quantity may be written as

$$n_{exc} = \sum_i \langle \rho_i \rangle \Delta H_i \left(\frac{dV}{dH}\right)_i - \frac{\rho_{bulk} H_{He_i}}{H_i} \Delta H_i \left(\frac{dV}{dH}\right)_i, \tag{37}$$

where $\langle \rho_i \rangle$ is the average density in the pore given by $\langle \rho_i \rangle = \frac{1}{H_i} \int_0^{H_i} \rho(z) dz$, H_i is the size of pore i. ΔH_i and $(dV/dH)_i$ are the width of pore sizes corresponding to the pores of the region i of the selected discretization and the maximum value of the PSD function at H_i, respectively (see Figure 6). ρ_{bulk} is the bulk density of methane at considered temperature and pressure and H_{Hei} is the effective pore width accessible to the fluid having the "Helium calibrated" pore volume determined by $H'_{Hei} = H_i - 2 \times 0.71^*(\sigma_{ss} + \sigma_{He})/2$ with $\sigma_{He} = 0.26$ nm.

The fluid and solid molecular parameters are the same as previously used except for ε_{ss} because the Carboxen 1012 is not strictly made of carbon but also have few other components (oxygen, etc.). To correct this, we have fitted ε_{ss} at a given pressure to obtain the best representation of the

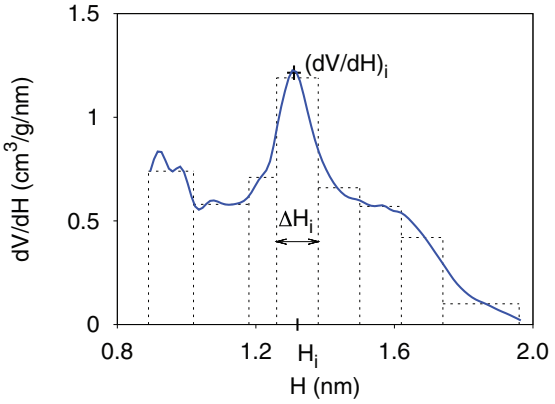

FIG. 6. Pore size distribution of Carboxen 1012 obtained from the experimental N_2 adsorption isotherm at 77.4 K and its discretization. Each category of micropores i is defined by a width ΔH_i centered in H_i and a value of the variation of the volume with respect to the pore at i $(dV/dH)_i$.

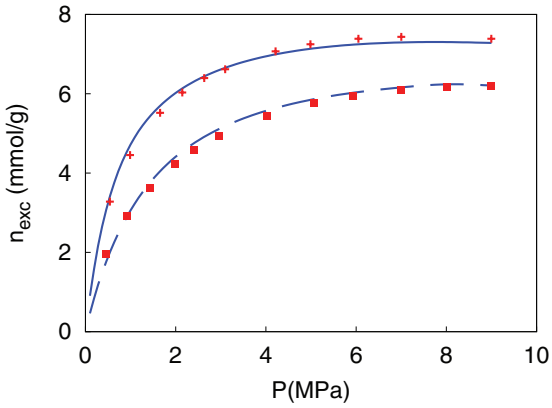

FIG. 7. Adsorption isotherm of methane in Carboxen 1012. The continuous and dotted curves are modelling results at 313 K and 353 K, respectively, from the "CG" version of the NLDFT/SAFT-VR theory. Crosses and squares are experimental points at 313 K and 353 K, respectively.

experimental adsorption isotherm at 313 K and we have transferred this value for all the other pressures and temperatures. The final value obtained, $\varepsilon_{ss}/k_B = 35$ K, is a reasonable value in comparison with previous works on DFT and activated carbons,[58] where $\varepsilon_{ss}/k_B \approx 30$ K. Figure 7 shows the modeled and experimental adsorption isotherms of methane on Carboxen 1012 at two different temperatures and a wide range of pressures. As it can be seen, the model proposed is able to describe the adsorbed amount of methane on the porous material at every thermodynamic condition without any further adjustment. The excellent agreement between theoretical and experimental results proves the consistency of both the characterization and the modeling and their ability to reproduce methane adsorption isotherms on Carboxen 1012.

IV. CONCLUSIONS

In this study, we have built a new theoretical model to describe fluids of monomers in highly confined media. We have developed an original NLDFT/SAFT-VR coupling in order to take into account the inhomogeneities in the fluid. The MFMT was used, as done in previous DFT studies, to describe the hard sphere Helmholtz free energy contribution. Two methods were then probed to express the dispersive terms. One used the weighted densities from the FMT for these contributions and the other used a CG approach to describe the density in a non-local fashion. Density profiles of methane as the monomer fluid in carbon slit micropores were compared to GCMC calculations and the "CG" method was found to be in excellent agreement whereas the "FMT" approach has underestimated the density in the pores. Thus, the "CG" approach was used to generate a capillary condensation transition and its hysteresis as well as the equilibrium transition in a mesopore in excellent agreement with GCMC simulations. Finally, The "CG" approach was applied to generate methane adsorption isotherms in Carboxen 1012 and the comparison with experimental results, through a correct characterization of the material, has shown again the accuracy of the model proposed herein. Thus, through a complete and consistent comparison both with molecular simulations and experimental data, the

NLDFT/SAFT-VR theory has been validated for monomers description. In summary, the new molecular-based theory presented in this work seems to be an accurate formalism to predict the structural and thermodynamic properties of simple molecules adsorbed on porous materials at any condition of temperature and pressure. Since the formalism is based on the combination of DFT and SAFT, in which the contributions to different microscopic effects are clearly separated and described accurately, this work is the theoretical base for the extension of the formalism to deal with the adsorption behaviour of more complex fluids. In a future work, we will extend the theory proposed here to predict adsorption properties of chainlike and associating molecules of industrial interest on porous materials.

ACKNOWLEDGMENTS

This work was sponsored by the ERC advanced grant Failflow (27769). This financial support is gratefully acknowledged. This work was supported by Acción Integrada España-Francia from Ministerio de Ciencia e Innovación and Picasso Project (Project Nos. FR2009-0056 and PHC PICASSO2010). F.J.B. would like to acknowledge financial support from Ministerio de Ciencia e Innovacación (Project No. FIS2010-14866), Junta de Andalucía, and Universidad de Huelva.

C. Malheiro would like to acknowledge the ISIFOR Carnot institute for her mobility grant.

[1]K. R. Matranga, A. L. Myers, and E. D. Glandt, Chem. Eng. Sci. **47**, 1569 (1992).
[2]Z. Yang, Y. Xia, and Y. Zhu, Mater. Chem. Phys. **141**, 318 (2013).
[3]G. G. Santillán-Reyes and H. Pfeiffer, Int. J. Greenhouse Gas Control **5**, 1624 (2011).
[4]F. Zhou, F. Hussain, and Y. Cinar, Int. J. Coal Geol. **116–117**, 53 (2013).
[5]R. Evans, in *Fundamentals of Inhomogeneous Fluids*, edited by D. Henderson (Marcel Dekker, New York, 1992), p. 85.
[6]J. Wu and Z. Li, Annu. Rev. Phys. Chem. **58**, 85 (2007).
[7]J. Wu, AIChE J. **52**, 1169 (2006).
[8]C. P. Emborsky, Z. Feng, K. R. Cox, and W. G. Chapman, Fluid Phase Equilib. **306**, 15 (2011).
[9]J. Landers, G. Y. Gor, and A. V. Neimark, Colloids Surf., A **437**, 3 (2013).
[10]H. T. Davis, *Statistical Mechanics of Phases, Interfaces, and Thin Films* (VCH, 1996).
[11]M. S. Wertheim, J. Stat. Phys. **35**, 19 (1984).
[12]M. S. Wertheim, J. Stat. Phys. **35**, 35 (1984).
[13]W. G. Chapman, K. E. Gubbins, G. Jackson, and M. Radosz, Fluid Phase Equilib. **52**, 31 (1989).
[14]W. G. Chapman, K. E. Gubbins, G. Jackson, and M. Radosz, Ind. Eng. Chem. Res. **29**, 1709 (1990).
[15]F. J. Blas, E. M. Del Río, E. De Miguel, and G. Jackson, Mol. Phys. **99**, 1851 (2001).
[16]G. J. Gloor, F. J. Blas, E. M. Del Río, E. De Miguel, and G. Jackson, Fluid Phase Equilib. **194–197**, 521 (2002).
[17]G. J. Gloor, G. Jackson, F. J. Blas, E. M. Del Río, and E. de Miguel, J. Chem. Phys. **121**, 12740 (2004).
[18]G. J. Gloor, G. Jackson, F. J. Blas, E. M. del Río, and E. de Miguel, J. Phys. Chem. C **111**, 15513 (2007).
[19]F. Llovell, A. Galindo, F. J. Blas, and G. Jackson, J. Chem. Phys. **133**, 024704 (2010).
[20]F. Llovell, N. Mac Dowell, F. J. Blas, A. Galindo, and G. Jackson, Fluid Phase Equilib. **336**, 137 (2012).
[21]H. Kahl and J. Winkelmann, Fluid Phase Equilib. **270**, 50 (2008).
[22]A. von Müller and K. Leonhard, Fluid Phase Equilib. **356**, 96 (2013).
[23]Y. Rosenfeld, Phys. Rev. Lett. **63**, 980 (1989).
[24]R. Roth, J. Phys. Condens. Matter **22**, 063102 (2010).
[25]Y.-X. Yu and J. Wu, J. Chem. Phys. **117**, 10156 (2002).
[26]J. B. Schulte, P. A. Kreitzberg, C. V. Haglund, and D. Roundy, Phys. Rev. E **86**, 061201 (2012).
[27]Y.-X. Yu and J. Wu, J. Chem. Phys. **116**, 7094 (2002).
[28]P. Bryk, S. Sokołowski, and O. Pizio, J. Chem. Phys. **125**, 024909 (2006).
[29]J. Gross, J. Chem. Phys. **131**, 204705 (2009).
[30]X. Xu, D. E. Cristancho, S. Costeux, and Z.-G. Wang, J. Chem. Phys. **137**, 054902 (2012).
[31]J. Hughes, E. J. Krebs, and D. Roundy, J. Chem. Phys. **138**, 024509 (2013).
[32]Z. Ye, J. Cai, H. Liu, and Y. Hu, J. Chem. Phys. **123**, 194902 (2005).
[33]Z. Ye, H. Chen, H. Liu, Y. Hu, and J. Jiang, J. Chem. Phys. **126**, 134903 (2007).
[34]G. Shen, X. Ji, and X. Lu, J. Chem. Phys. **138**, 224706 (2013).
[35]G. Shen, X. Ji, S. OÖberg, and X. Lu, J. Chem. Phys. **139**, 194705 (2013).
[36]B. J. Schindler, L. A. Mitchell, C. McCabe, P. T. Cummings, and M. D. LeVan, J. Phys. Chem. C **117**, 21337 (2013).
[37]S. Tripathi and W. G. Chapman, J. Chem. Phys. **122**, 094506 (2005).
[38]A. Dominik, S. Tripathi, and W. G. Chapman, Ind. Eng. Chem. Res. **45**, 6785 (2006).
[39]S. Jain, A. Dominik, and W. G. Chapman, J. Chem. Phys. **127**, 244904 (2007).
[40]A. Bymaster, A. Dominik, and W. G. Chapman, J. Phys. Chem. C **111**, 15823 (2007).
[41]A. Gil-Villegas, A. Galindo, P. J. Whitehead, S. J. Mills, G. Jackson, and A. N. Burgess, J. Chem. Phys. **106**, 4168 (1997).
[42]J. A. Barker and D. Henderson, J. Chem. Phys. **47**, 2856 (1967).
[43]J. A. Barker and D. Henderson, J. Chem. Phys. **47**, 4714 (1967).
[44]R. Roth, R. Evans, A. Lang, and G. Kahl, J. Phys. Condens. Matter **14**, 12063 (2002).
[45]N. F. Carnahan and K. E. Starling, J. Chem. Phys. **51**, 635 (1969).
[46]M. C. dos Ramos, H. Docherty, F. J. Blas, and A. Galindo, Fluid Phase Equilib. **276**, 116 (2009).
[47]J. K. Percus and G. J. Yevick, Phys. Rev. **110**, 1 (1958).
[48]H. Hansen-Goos and R. Roth, J. Phys. Condens. Matter **18**, 8413 (2006).
[49]P. Tarazona, Phys. Rev. A **31**, 2672 (1985).
[50]Z. Tan and K. Gubbins, J. Phys. Chem. **94**, 6061 (1990).
[51]W. A. Steele, Surf. Sci. **36**, 317 (1973).
[52]E. De Miguel and G. Jackson, Mol. Phys. **104**, 3717 (2006).
[53]C. McCabe and G. Jackson, Phys. Chem. Chem. Phys. **1**, 2057 (1999).
[54]F. Khaddour, A. Knorst-Fouran, F. Plantier, M. M. Piñeiro, B. Mendiboure, and C. Miqueu, "A fully consistent experimental and molecular simulation study of methane adsorption on activated carbon," Adsorption (in press).
[55]S. V. Mikhalovsky, V. V. Turov, R. Leboda, and W. R. Betz, Adsorption **11**, 657 (2005).
[56]C. Malheiro, B. Mendiboure, F. Plantier, B. Guatarbes, and C. Miqueu, "An accurate model for the filling pressure of carbon slit-like micropores: Application to the pore size distribution calculation" (unpublished).
[57]G. Horvath and K. Kawazoe, J. Chem. Eng. Jpn. **16**, 470 (1983).
[58]C. Lastoskie, K. E. Gubbins, and N. Quirke, J. Phys. Chem. **97**, 4786 (1993).